ADVANCED MATERIALS

Supporting Information

for *Adv. Mater.,* DOI: 10.1002/adma.202205154

Immune Profiling and Multiplexed Label-Free Detection of 2D MXenes by Mass Cytometry and High-Dimensional Imaging

Laura Fusco, Arianna Gazzi, Christopher E. Shuck, Marco Orecchioni, Dafne Alberti, Sènan Mickael D'Almeida, Darawan Rinchai, Eiman Ahmed, Ofer Elhanani, Martina Rauner, Barbara Zavan, Jean-Charles Grivel, Leeat Keren, Giulia Pasqual, Davide Bedognetti, Klaus Ley, Yury Gogotsi, and Lucia Gemma Delogu**

Supplementary Information for

Immune Profiling and Multiplexed Label-Free Detection of 2D MXenes by Mass Cytometry and High-Dimensional Imaging

Laura Fusco[#], Arianna Gazzi[#], Christopher E. Shuck, Marco Orecchioni, Dafne Alberti, Sènan Mickael D'Almeida, Darawan Rinchai, Eiman Ahmed, Ofer Elhanani, Martina Rauner, Barbara Zavan, Jean-Charles Grivel, Leeat Keren, Giulia Pasqual, Davide Bedognetti, Klaus Ley, Yury Gogotsi* & Lucia Gemma Delogu*

[#]equal contribution

[*]corresponding authors

L. Fusco, A. Gazzi, L.G. Delogu

ImmuneNano Laboratory, Department of Biomedical Sciences, University of Padua, Padua, 35129, Italy

Email: luciagemma.delogu@unipd.it

L. Fusco, C.E. Shuck, Y. Gogotsi

A. J. Drexel Nanomaterials Institute and Department of Materials Science and Engineering, Drexel University, Philadelphia, Pennsylvania, 19104, USA

Email: gogotsi@drexel.edu

L. Fusco, D. Rinchai, E. Ahmed, D. Bedognetti

Human Immunology Division, Translational Medicine Department, Sidra Medicine, Doha, 26999, Qatar

A. Gazzi

Department of Chemical and Pharmaceutical Sciences, University of Trieste, Trieste, 34127, Italy

M. Orecchioni, K. Ley

La Jolla Institute for Immunology, San Diego, CA, 92037, USA

D. Alberti, G. Pasqual
Laboratory of Synthetic Immunology, Oncology and Immunology Section, Department of Surgery Oncology and Gastroenterology, University of Padua, Padua, 35124, Italy

S.M. D'Almeida
Flow Cytometry Core Facility, School of Life Sciences, Ecole Polytechnique Fédérale de Lausanne (EPFL), 1015, Lausanne, Switzerland

O. Elhanani, L. Keren
Department of Molecular Cell Biology, Weizmann Institute of Science, Rehovot, 7610001, Israel

M. Rauner
Department of Medicine III, Center for Healthy Aging, Technical University Dresden, Dresden, 01307, Germany

B. Zavan
Department of Medical Sciences, University of Ferrara, Ferrara, 44121, Italy
Maria Cecilia Hospital, GVM Care & Research, Ravenna, 48033, Italy

J.C. Grivel
Deep Phenotyping Core, Sidra Medicine, Doha, 26999, Qatar

D. Bedognetti
Department of Internal Medicine and Medical Specialties, University of Genoa, Genoa, 16132, Italy
College of Health and Life Sciences, Hamad Bin Khalifa University, Doha, 34110, Qatar

K. Ley
Immunology Center of Georgia (IMMCG), Augusta University, Augusta, GA, 30912, USA

Keywords: biocompatibility, biomedical applications, detection, immune system, nanomedicine, MXenes

The supplementary information includes:

1. Supplementary Figures S1-S18 and Tables S1-S4

2. Materials and methods

3. Supplementary references

1. Supplementary Figures

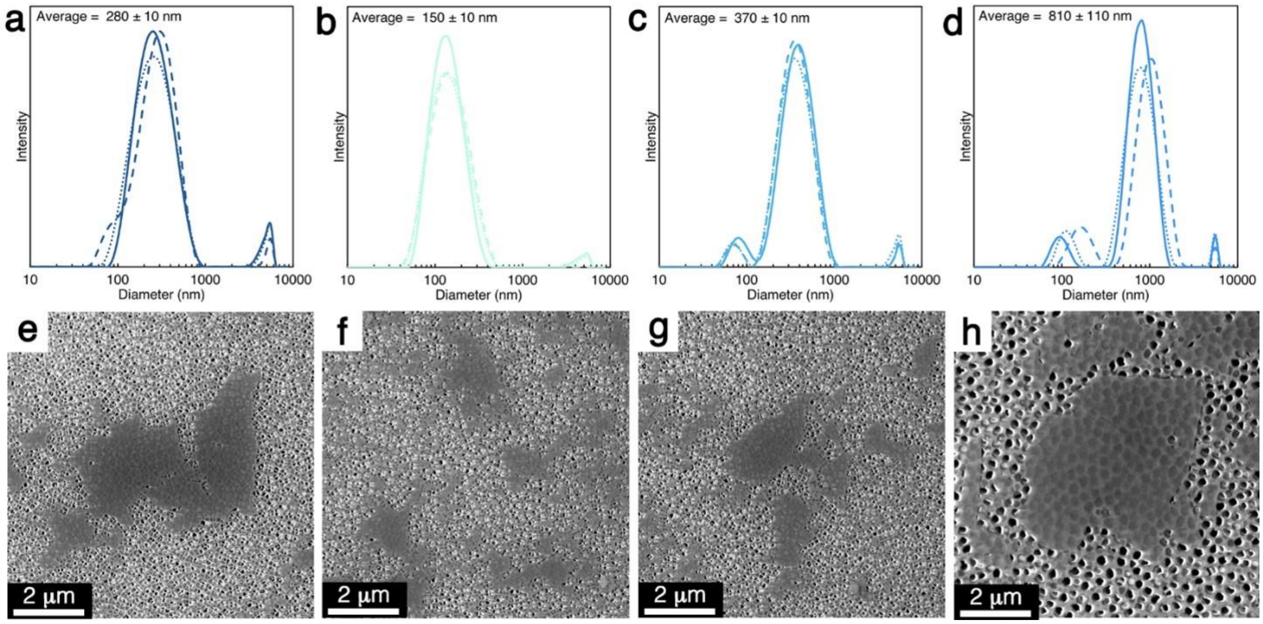

Figure S1. Material chemical characterization. a-d, Dynamic light scattering (DLS) of $Ti_3C_2T_x$ (**a**), $Nb_4C_3T_x$ **(b)**, $Mo_2Ti_2C_3T_x$ **(c)**, and $Ta_4C_3T_x$ **(d)** indicating their hydrodynamic radius. **e-h**, Scanning electron microscopy (SEM) images of $Ti_3C_2T_x$ (**e**), $Nb_4C_3T_x$ **(f)**, $Mo_2Ti_2C_3T_x$ **(g)**, and $Ta_4C_3T_x$ (h) showing the flake size and morphology after delamination.

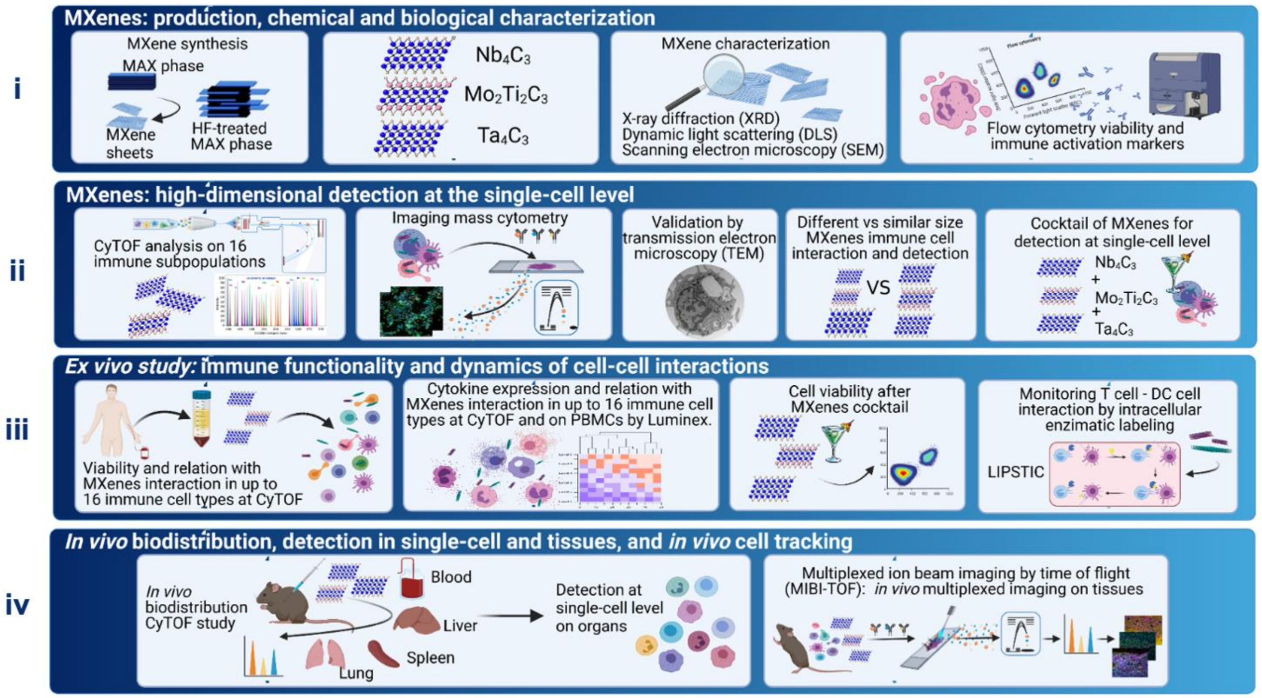

Figure S2. Study workflow. Study workflow showing synthesis and physical-chemical and basic biological characterization of MXenes (i); *ex vivo* assessment of MXene detection on 16 human immune cell types by single-cell mass cytometry and imaging mass cytometry, impact of lateral size and as a cocktail of MXenes (ii); evaluation of MXene effects on cell viability, cell functionality, and dynamics of cell-cell interactions by means of single-cell mass spectrometry and LIPSTIC approach[1] (iii); and *in vivo* MXene testing from biodistribution to *in vivo* cell tracking by single-cell mass cytometry and multiplexed ion beam imaging (iv) .

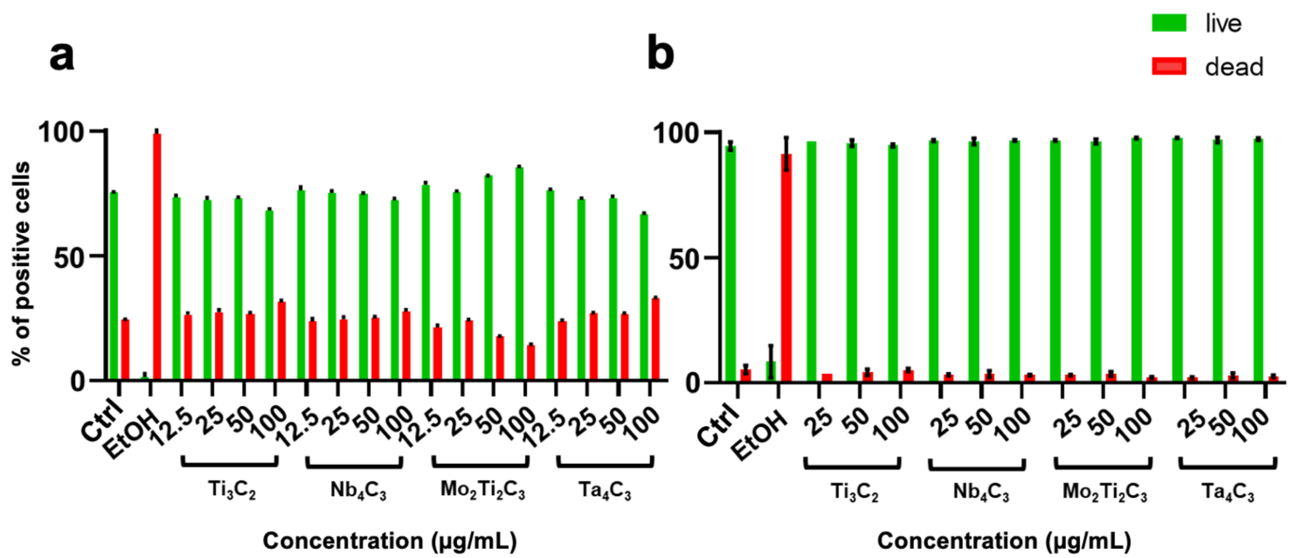

Figure S3. Impact of Ti_3C_2, Nb_4C_3, $Mo_2Ti_2C_3$, and Ta_4C_3 on human PBMC viability. a, PBMCs were treated with different concentrations (12.5, 25, 50, and 100 μg/mL) of Ti_3C_2, Nb_4C_3, $Mo_2Ti_2C_3$ or Ta_4C_3 for 24 h and cell viability was analysed using the LIVE/DEAD® Viability/Cytotoxicity Kit discriminating live from dead cells by simultaneously staining with green-fluorescent calcein-AM to indicate intracellular esterase activity and red-fluorescent ethidium homodimer-1 to indicate loss of plasma membrane integrity. Plasma membrane integrity and esterase activity were measured by using TECAN fluorescence microplate reader. **b**, PBMCs were treated with different concentrations (25, 50, and 100 μg/mL) of Ti_3C_2, Nb_4C_3, $Mo_2Ti_2C_3$ or Ta_4C_3 for 24 h and cell viability was analysed by flow cytometry using Fixable Viability Dye 780 staining. All the experiments were performed in triplicate and shown as means±SD (Two-way ANOVA, followed by Dunnett's multiple comparison test).

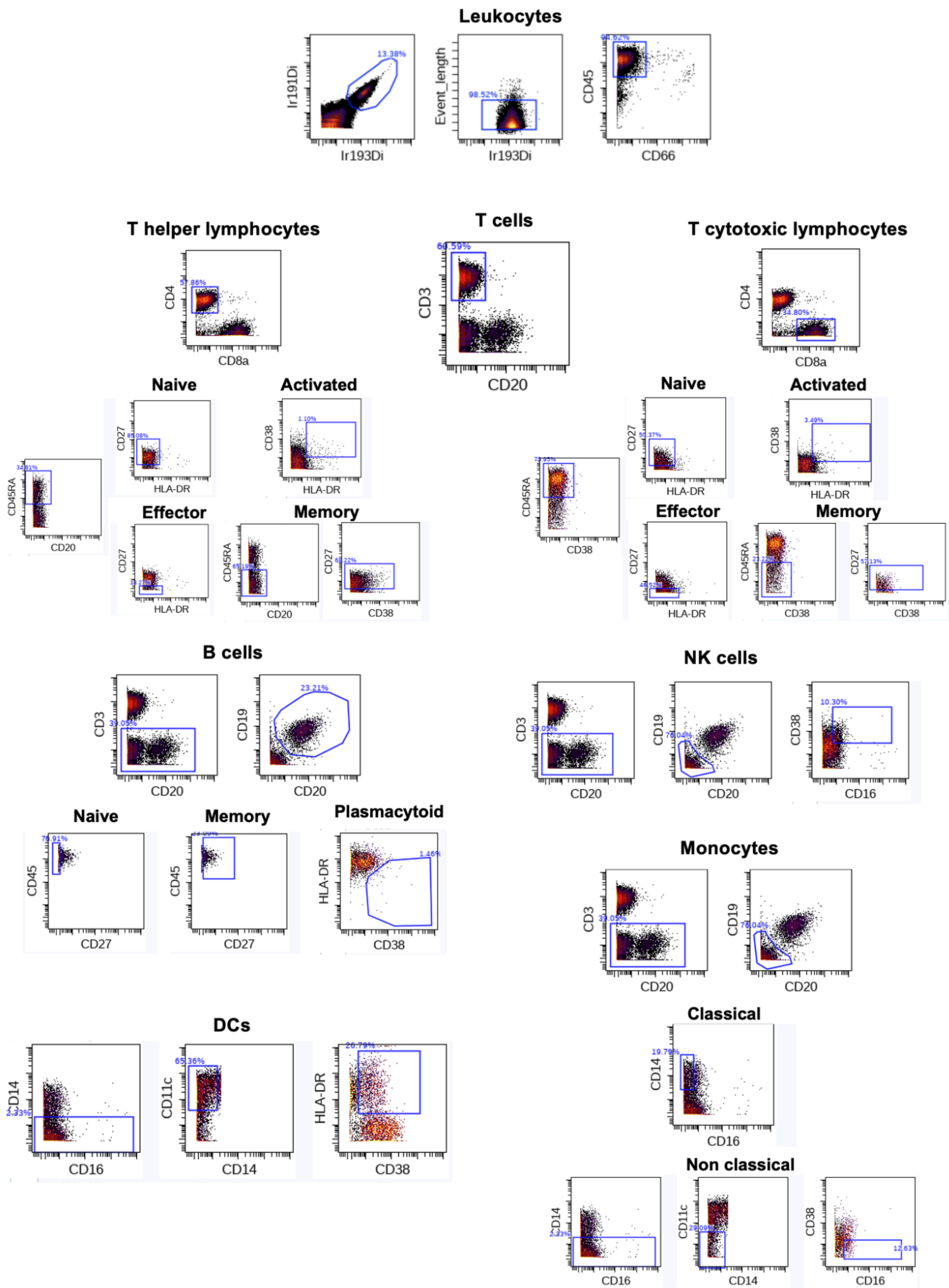
Leukocytes
Ir191Di
Ir193Di
13.38%
Event_length
Ir193Di
98.52%
CD45
CD66
T helper lymphocytes
CD4
CD8a
T cells
CD3
CD20
69.59%
T cytotoxic lymphocytes
CD4
CD8a
34.80%
Naive
Activated
CD45RA
CD20
CD27
HLA-DR
CD38
HLA-DR
Effector
Memory
CD27
HLA-DR
CD45RA
CD20
CD27
CD38
Naive
Activated
CD45RA
CD38
CD27
HLA-DR
CD38
HLA-DR
Effector
Memory
CD27
HLA-DR
CD45RA
CD38
CD27
CD38
B cells
CD3
CD20
CD19
CD20
23.21%
NK cells
CD3
CD20
CD19
CD20
CD38
CD16
10.30%
Naive
Memory
Plasmacytoid
CD45
CD27
CD45
CD27
HLA-DR
CD38
1.46%
Monocytes
CD3
CD20
CD19
CD20
DCs
CD14
CD16
CD11c
CD14
65.36%
HLA-DR
CD38
Classical
CD14
CD16
19.79%
Non classical
CD14
CD16
CD11c
CD14
CD38
CD16
12.63%

Figure S4. Immune cell subpopulations gating strategy. Dot plots showing the gating strategy used for the identification of the different immune cell subpopulations by CyTOF.

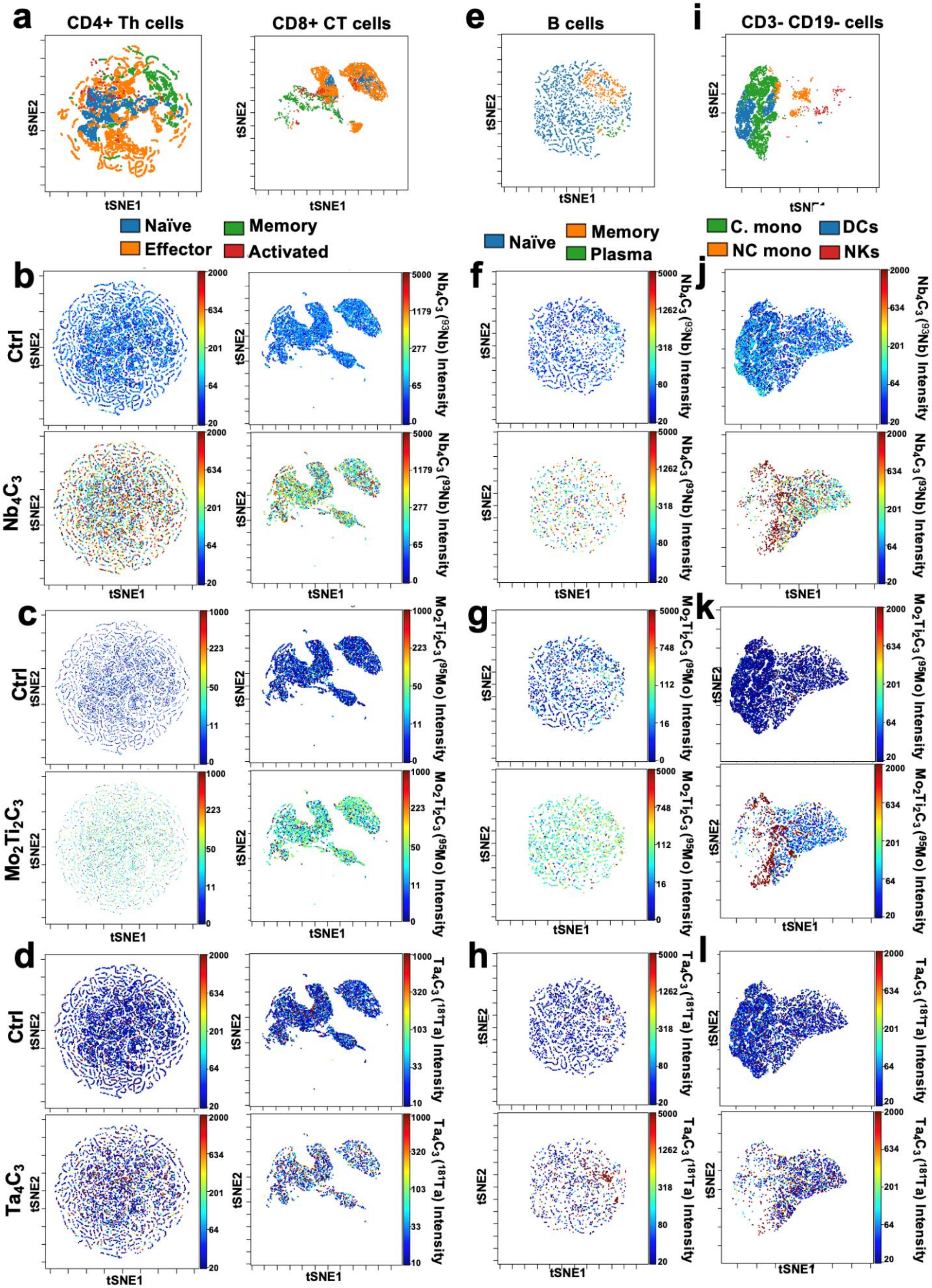
a
CD4+ Th cells
CD8+ CT cells
e
B cells
i
CD3- CD19- cells
tSNE1
tSNE2
Naïve
Effector
Memory
Activated
Naïve
Memory
Plasma
C. mono
NC mono
DCs
NKs
b
Ctrl
Nb_4C_3
Nb_4C_3 (^{93}Nb) Intensity
f
j
c
g
k
$Mo_2Ti_2C_3$
$Mo_2Ti_2C_3$ (^{95}Mo) Intensity
d
h
l
Ta_4C_3
Ta_4C_3 (^{181}Ta) Intensity

Figure S5. Single-cell tracking analysis of MXenes on human PBMC subpopulations. a-l, viSNE distribution of CD4+ Th. cells, CD8+ CT. cells (**a-d**), B cells (**e-h**) and CD3- CD19- cells (**i-l**). Plots representing the use of viSNE to obtain a comprehensive single-cell view of the PBMC subpopulations treated with Nb_4C_3, $Mo_2Ti_2C_3$ or Ta_4C_3. showing the median intensity of Niobium (^{93}Nb), Molybdenum (^{95}Mo) and Tantalum (^{181}Ta) signal in CD4+ Th. cells, CD8+ CT. cells, B cells, monocytes, mDCs, and NKs. A representative viSNE graph is shown out of three biological replicates.

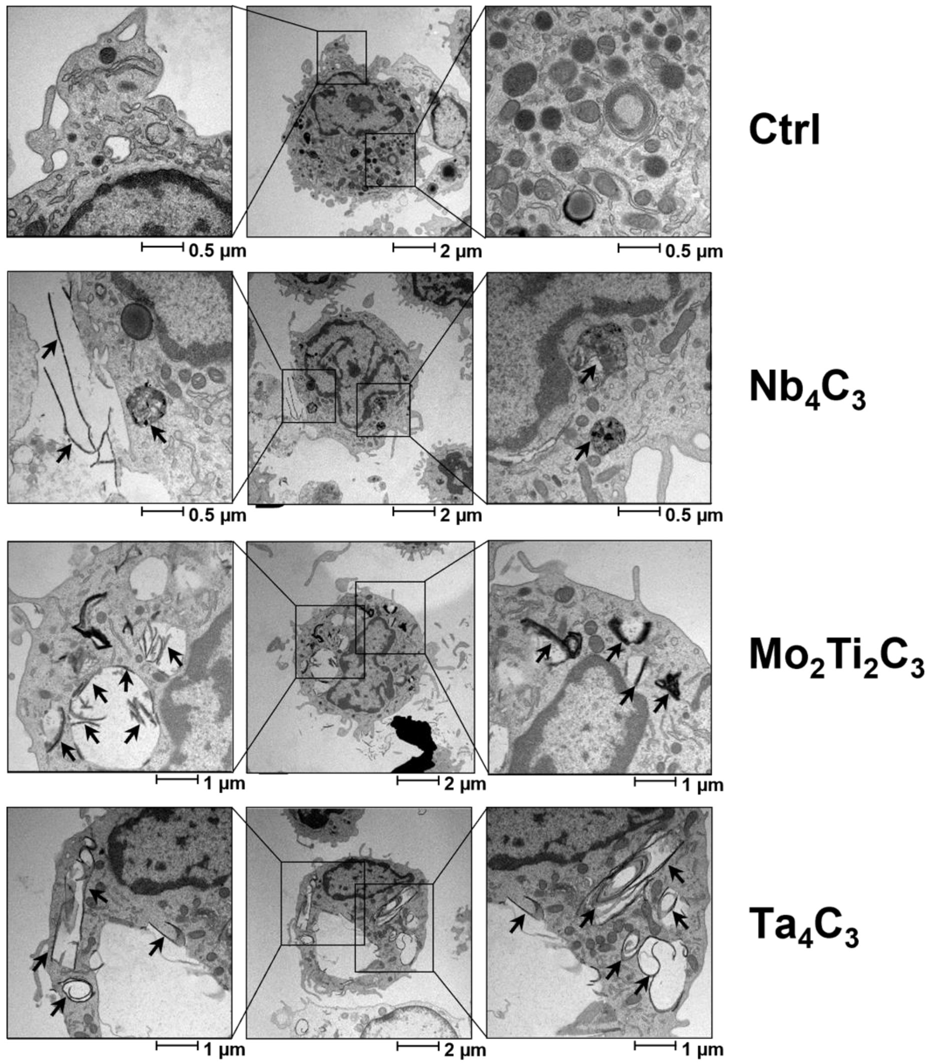

Figure S6. TEM Imaging. Representative TEM images of Nb_4C_3, $Mo_2Ti_2C_3$, and Ta_4C_3 interactions with PBMCs. Cells were incubated with Nb_4C_3, $Mo_2Ti_2C_3$ or Ta_4C_3 (50 µg/mL) for 24 h. Arrows in higher magnification micrographs indicate internalized Nb_4C_3, $Mo_2Ti_2C_3$, and Ta_4C_3. As shown in panel the representative images depict large aggregation and giant vacuoles inside the cells. Scale bars: 0.5, 1, and 2 µm.

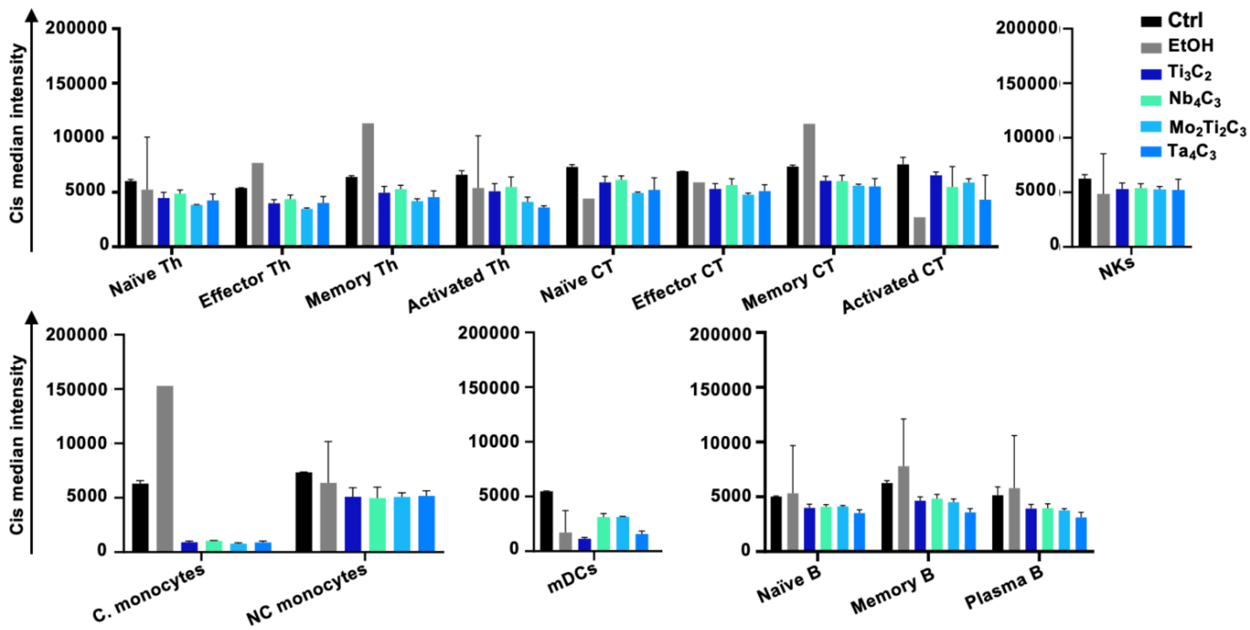

Figure S7. Single-cell impact of Ti_3C_2, Nb_4C_3, $Mo_2Ti_2C_3$, and Ta_4C_3 on PBMC viability. Histograms showing Cis median intensity in the different immune cell subpopulations after treatment with Ti_3C_2, Nb_4C_3, $Mo_2Ti_2C_3$ or Ta_4C_3 and analysed by CyTOF. All the experiments were performed in triplicate and shown as means±SD (Two-Way ANOVA and student T Test).

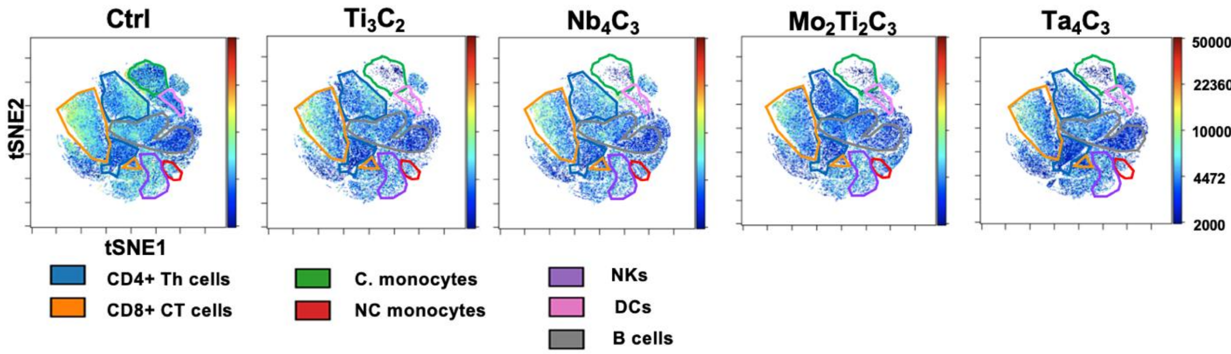

Figure S8. Analysis by t-SNE of cell viability upon MXene treatment on human PBMC subpopulations. PBMCs were treated with 50 µg/mL of Ti_3C_2, Nb_4C_3, $Mo_2Ti_2C_3$ or Ta_4C_3 for 24 h.

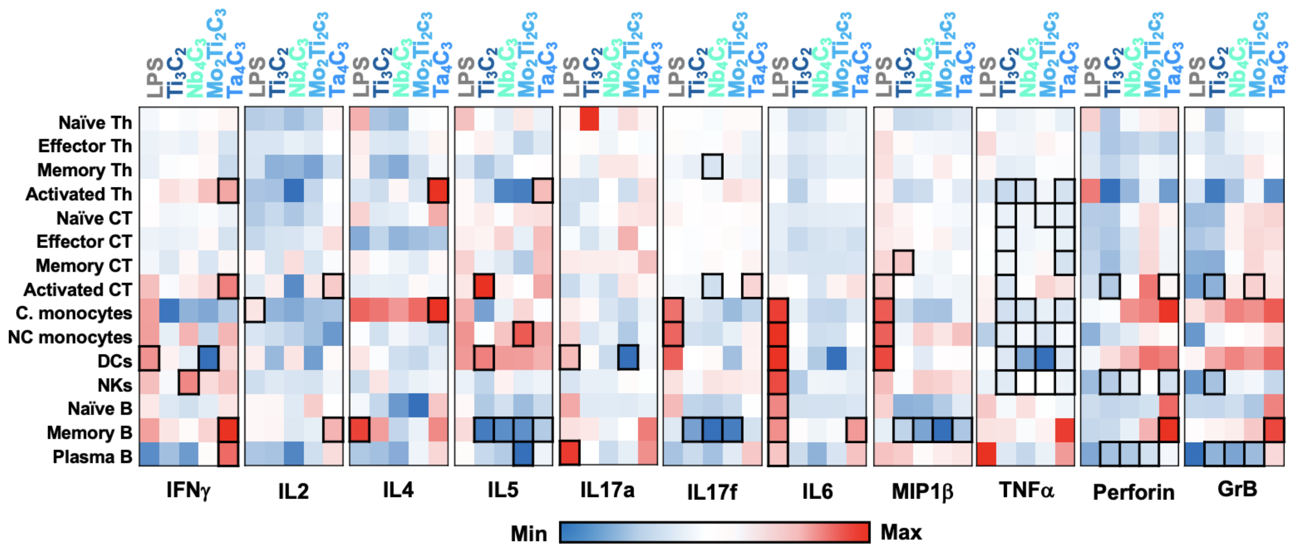

Figure S9. Single-cell cytokine analysis on human PBMC subpopulations. Heat maps showing median marker intensity of INFy, IL2, IL4, IL5, IL17a, IL17f, IL6, MP1β, TNFα, Perforin, and Granzyme B (GrB) for gated immune cell subpopulations after treatment of PBMCs with 50 μg/mL of Ti_3C_2, Nb_4C_3, $Mo_2Ti_2C_3$ or Ta_4C_3 for 24 h. Upregulated (red squares) or downregulated (blue squares) proteins are indicated. Significantly modulated values are marked as bold squares. All the experiments were performed in triplicate and shown as Log_2 Fold Change as compared to the negative control (Two-way ANOVA and Bonferroni post-test).

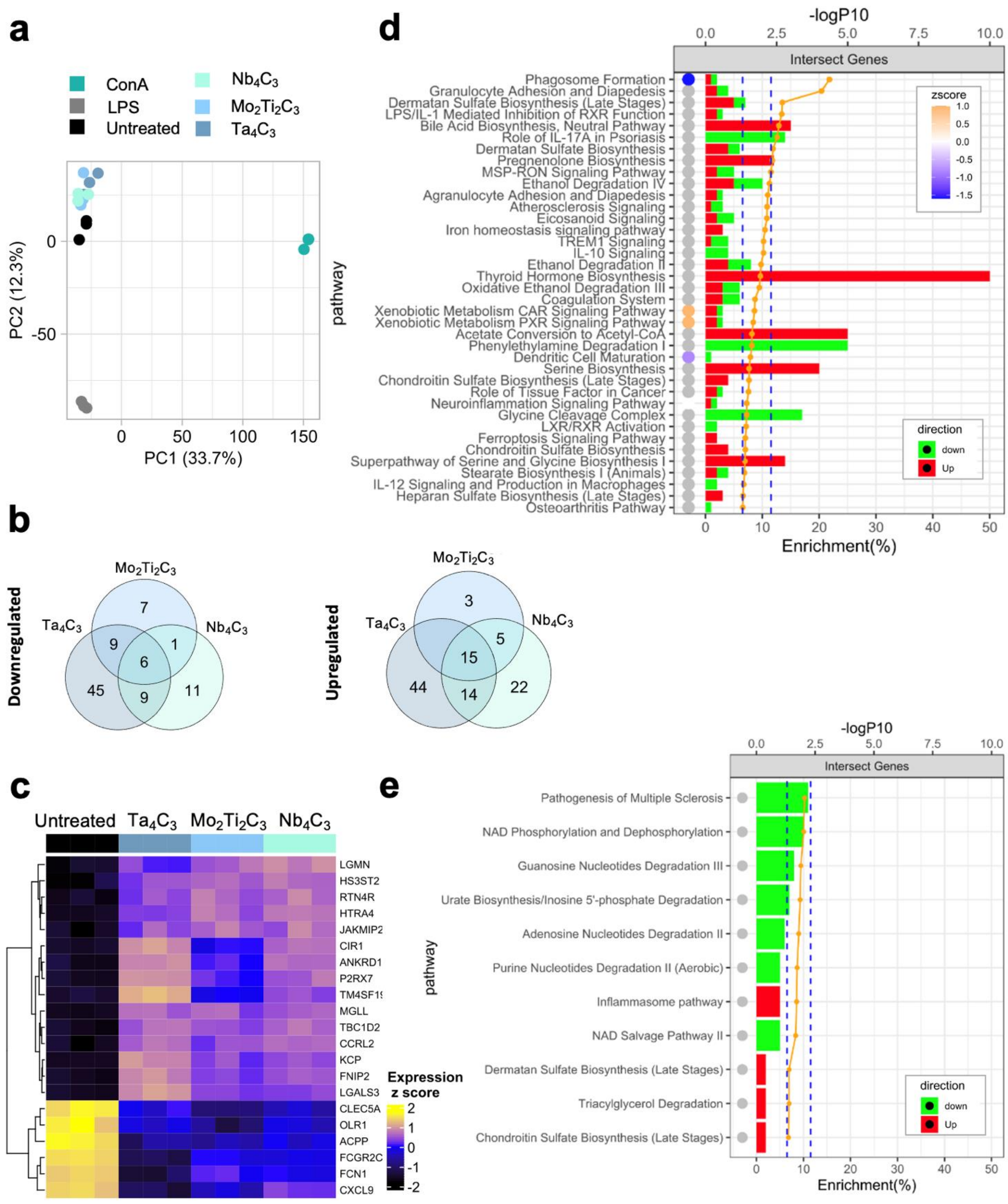

Figure S10. Gene expression analysis (RNA-seq on PBMCs). a, Principal component analysis based on the PBMC full normalized RNA-seq gene expression matrix. **b**, VennDiagram of differentially expressed genes using FDR < 0.01. **c**, Heatmap of differentially expressed genes (n

= 21) common to Ta_4C_3, $Mo_2Ti_2C_3$, and Nb_4C_3 using FDR < 0.01, as represented in panel b. **c,d,** Enriched pathways associated with DEGs common to Ta_4C_3, $Mo_2Ti_2C_3$, and Nb_4C_3 using FDR < 0.05 (**d**) and FDR < 0.01 (**e**). Experiments are performed in triplicates. Genes raw count data was normalized with EDAseq followed by quantile normalization and log2 transformation. Differentially expression analysis was performed using LIMMA. Enriched IPA canonical pathways using deferentially expressed genes coherently modulated by Ta_4C_3, $Mo_2Ti_2C_3$, and Nb_4C_3 vs controls with FDR < 0.05 (d) and FDR < 0.01 (e); enrichment *p* value is represented by the orange line, dotted lines represent two *p* values cut-offs ($p = 0.05 = -\text{Log}_{10}(p) = 1.3$, and 0.005, $-\text{Log}_{10}(p) = 2.3$). Histograms represent the proportion (%) of DEG upregulated (red) or downregulated (green) between MXenes and controls. The circles represent the inferred activation state. The bases of this inferred activation state are literature-derived relationships between genes and the corresponding biological function. Pathways that are activated in MXenes vs controls are marked with a red circle, indicating a positive activation score, whereas pathways inhibited in MXenes vs controls are marked with a blue circle, indicating a negative activation score. For canonical pathways with a gray circle, no sufficient literature-derived information exists to estimate the activation state.

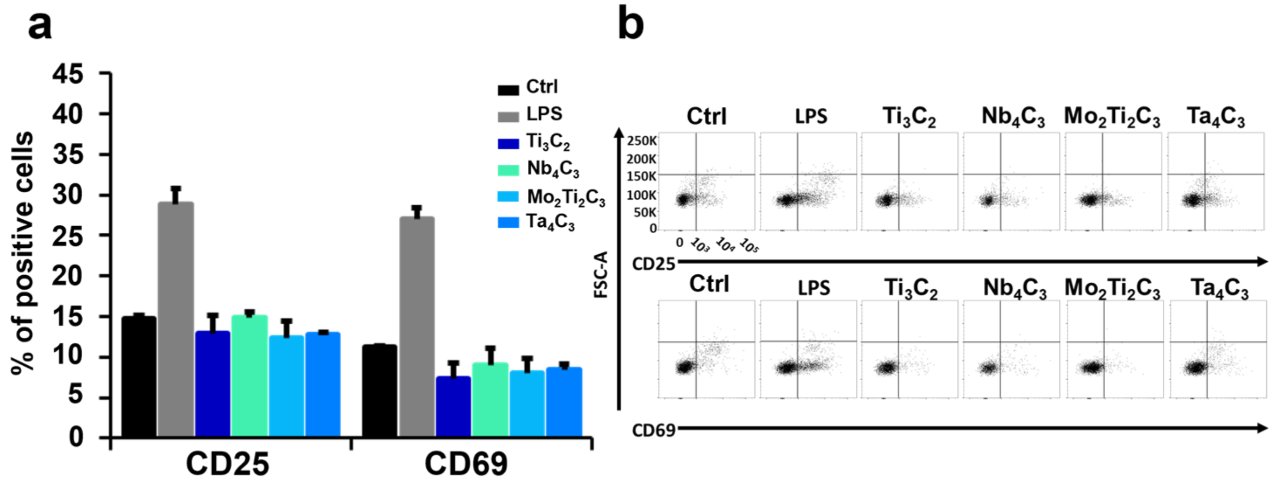

Figure S11. Analysis of PBMC activation. a, Histogram plots showing the percentage of positive cells for CD25-PE and CD69-FITC staining evaluated by flow cytometry in PBMCs treated with 50 µg/mL of Ti_3C_2, Nb_4C_3, $Mo_2Ti_2C_3$ or Ta_4C_3 for 24 h. LPS (2 µg/mL) was used as positive control. **b**, Representative flow cytometry analysis for CD25-PE and CD69-FITC staining of PBMCs and monocytes treated with 50 µg/mL of Ti_3C_2, Nb_4C_3, $Mo_2Ti_2C_3$ or Ta_4C_3. All the experiments were performed in triplicate and shown as means±SD (One-way ANOVA, followed by Tukey's post hoc multiple comparison).

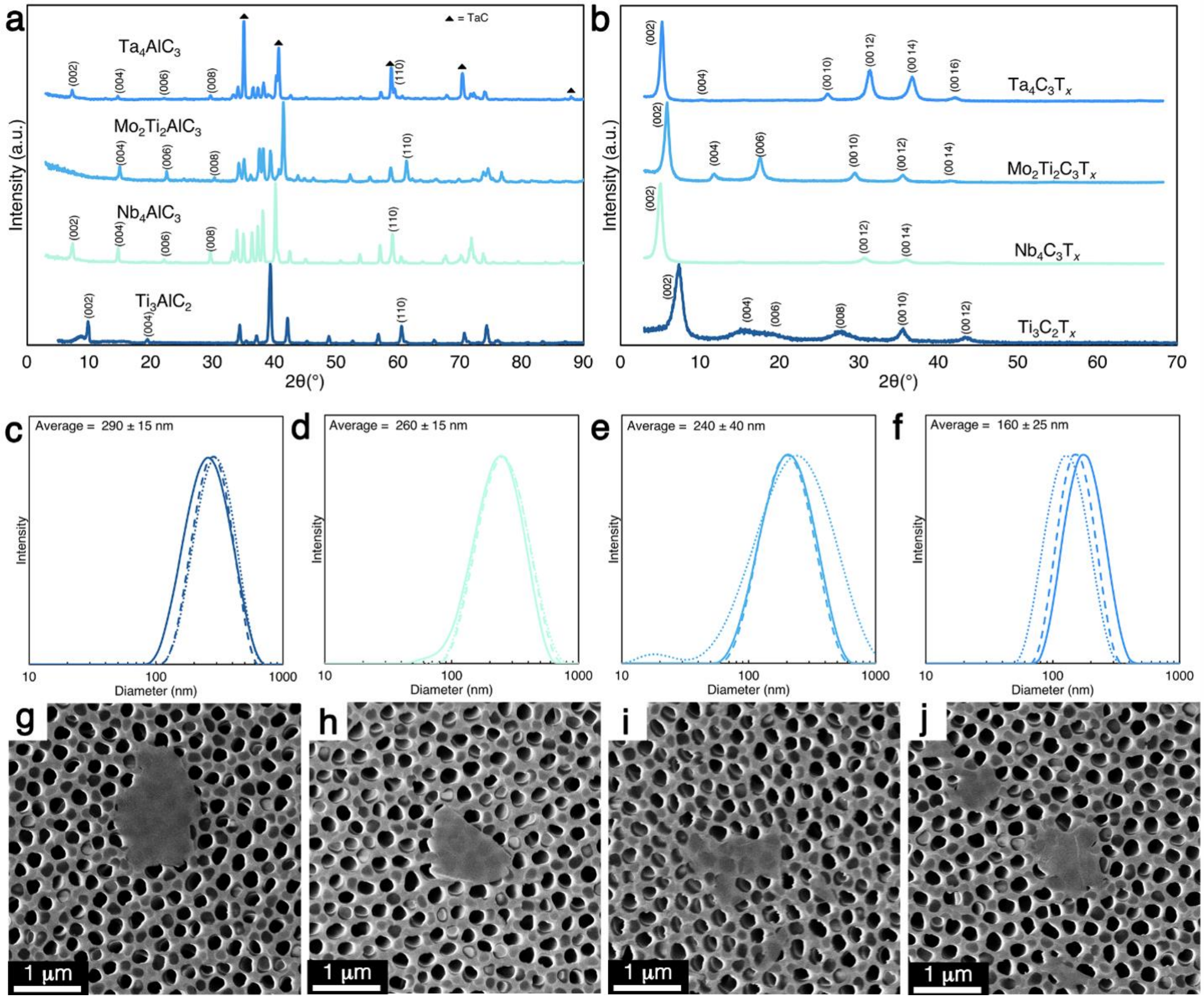

Figure S12. Characterization of MXenes with similar lateral size. a,**b**, X-ray diffraction (XRD) of precursor MAX phases (**a**) and MXenes (**b**) after topochemical synthesis. The (002) peak shifts to the left, and only (00*l*) peaks remain, indicating successful synthesis and delamination. **c-f**, Dynamic light scattering (DLS) of $Ti_3C_2T_x$ (**c**), $Nb_4C_3T_x$ (**d**), $Mo_2Ti_2C_3T_x$ (**e**), and $Ta_4C_3T_x$ (**f**) indicating their hydrodynamic radius. **g-j**, Scanning electron microscopy (SEM) images of $Ta_4C_3T_x$ (**g**), $Mo_2Ti_2C_3T_x$ (**h**), $Nb_4C_3T_x$ (**i**), and $Ti_3C_2T_x$ (**j**) showing the flake size and morphology after delamination.

a

MXenes	Nb_4C_3	$Mo_2Ti_2C_3$	Ta_4C_3
Av. lateral size (nm)	260	240	160
Ionization Energy	6.7589	7.0924	7.5496
C-O (%)	0	0	0
# of detectable atoms	3 x 10^6	2.6 x 10^6	1.1 x 10^6

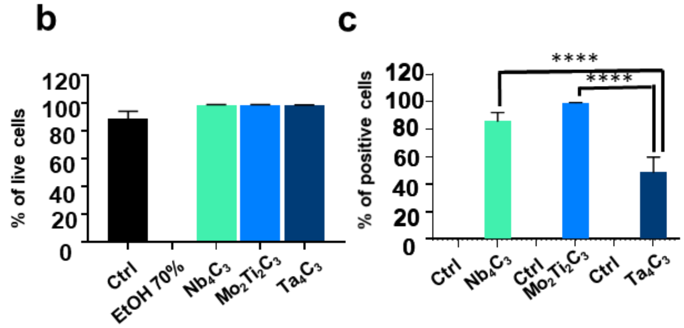

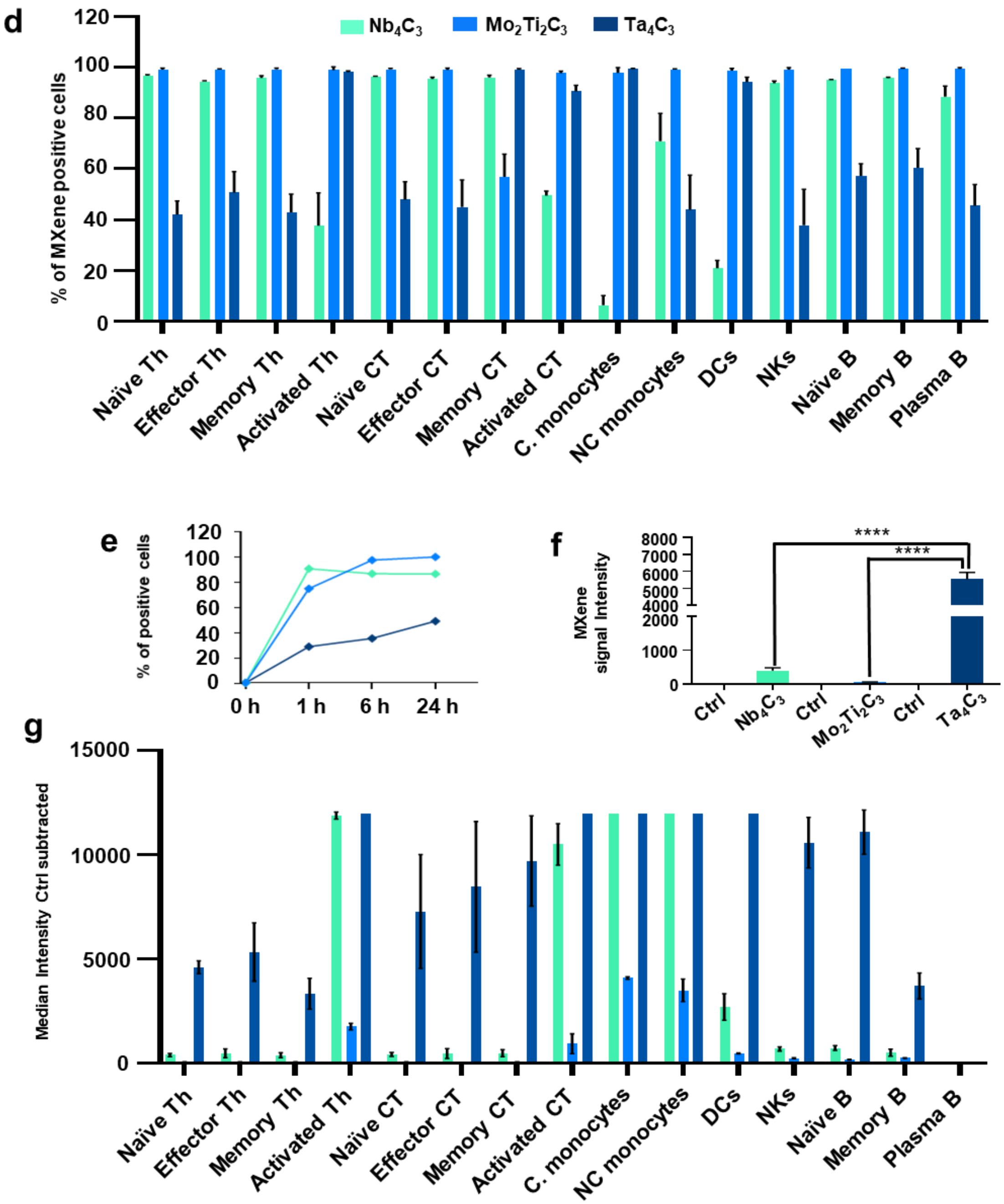

Figure S13. CyTOF detection of MXenes with similar lateral size in human immune cells. a, Table showing the main physicochemical characteristics of MXenes with similar lateral size (Nb_4C_3-260 nm, $Mo_2Ti_2C_3$-240 nm, and Ta_4C_3-160 nm). **b-g**, PBMCs were incubated with 50 µg/mL of Nb_4C_3-260 nm, $Mo_2Ti_2C_3$-240 nm or Ta_4C_3-160 nm and stained for mass cytometry analysis. Cell viability after 24 h was analysed using Cisplatin (Cis) reagent by CyTOF (**b**). Percentage of cells positive to Nb_4C_3, $Mo_2Ti_2C_3$ or Ta_4C_3 is reported as bar graphs for total PBMCs (**c**) and all PBMC subpopulations identified (**d**). Time course of MXenes uptake in PBMCs treated for 1, 6, and 24 h **(e)**. **f,g**, Median intensity of Nb_4C_3-260 nm, $Mo_2Ti_2C_3$-240 nm, and Ta_4C_3-160 nm signals after 24 h is also reported as histogram for total PBMCs (**f**) and all populations **(g)**. All the experiments were performed in triplicate and shown as means±SD. Statistical significance: **** $p<0.0001$ (One-way ANOVA, followed by Tukey's post hoc multiple comparison).

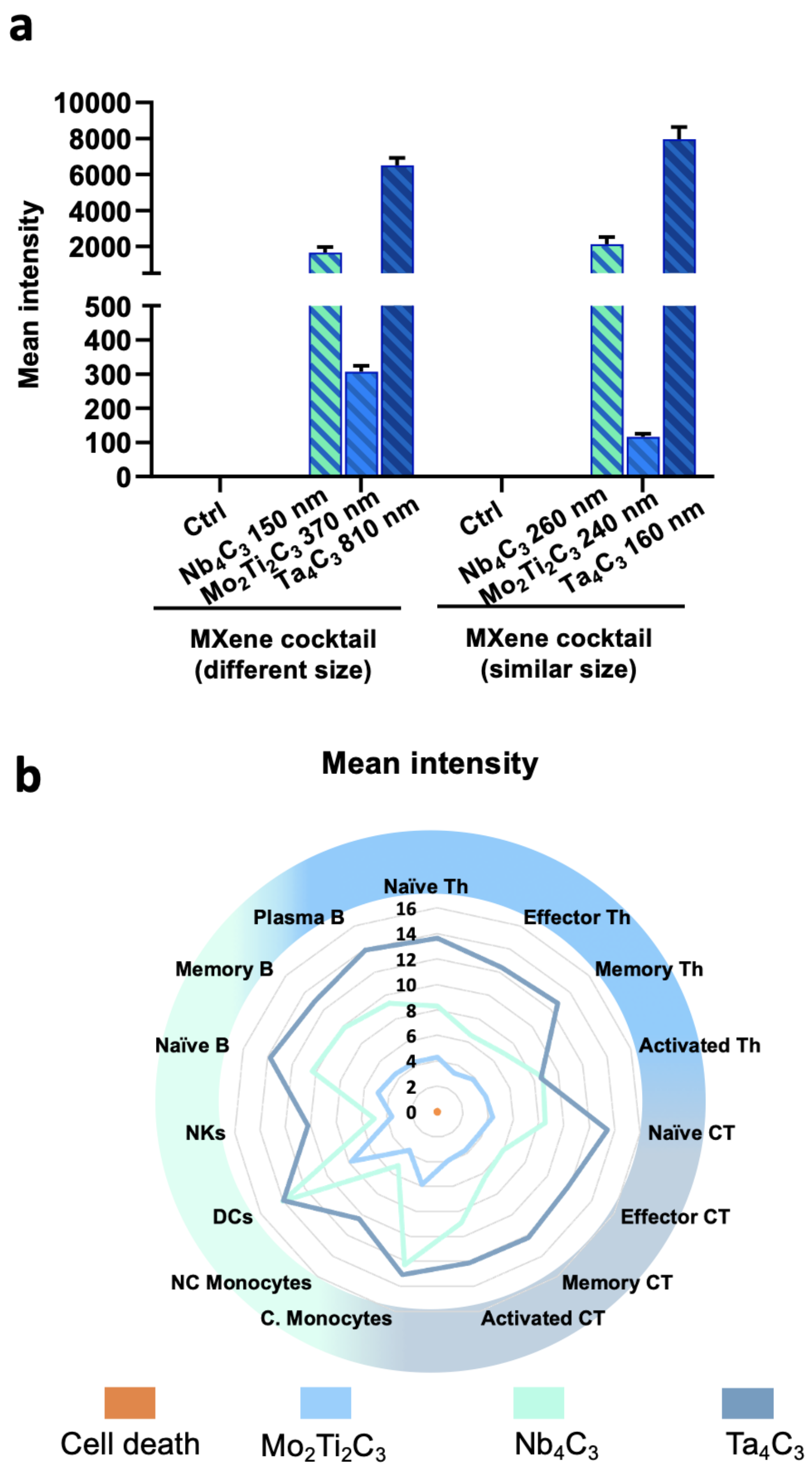

Figure S14. MXene cocktail on human PBMCs: viability and detection. a,b, PBMCs were incubated with a cocktail of Nb_4C_3-260 nm, $Mo_2Ti_2C_3$-240 nm, and Ta_4C_3-160 nm (50 µg/mL each) for 24 h and stained for mass cytometry analysis. Histograms representing the mean intensity of MXenes in total PBMCs after treatment for 24 h with the cocktail of MXenes with different size

(Nb_4C_3-150 nm, $Mo_2Ti_2C_3$-370 nm, and Ta_4C_3-810 nm; 50 µg/mL each) or similar size (Nb_4C_3-260 nm, $Mo_2Ti_2C_3$-240 nm, and Ta_4C_3-160 nm; 50 µg/mL each) (**a**). Detection on immune cell types was analysed by CyTOF. Spider chart represents the impact on viability (orange), expressed as LD median intensity for dead cells vs the MXene detection in fifteen immune cell types expressed as $\log_2$ fold change of mean intensity (**b**). All the experiments were performed in triplicate and shown as means±SD (One-way ANOVA, followed by Tukey's post hoc multiple comparison).

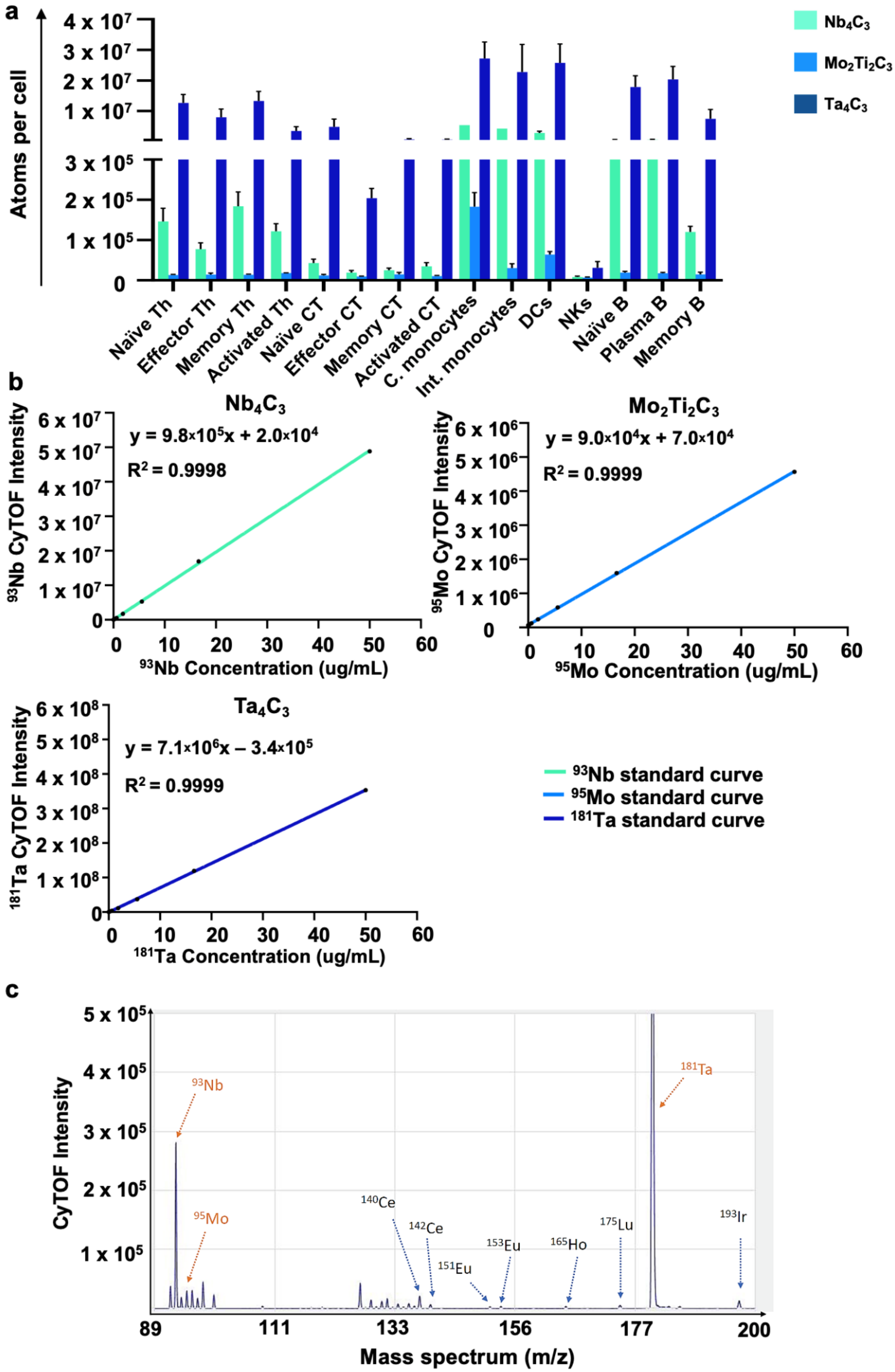
a
Atoms per cell
4 x 10^7
3 x 10^7
2 x 10^7
1 x 10^7
3 x 10^5
2 x 10^5
1 x 10^5
0
Nb4C3
Mo2Ti2C3
Ta4C3
Naïve Th
Effector Th
Memory Th
Activated Th
Naïve CT
Effector CT
Memory CT
Activated CT
C. monocytes
Int. monocytes
DCs
NKs
Naïve B
Plasma B
Memory B
b
Nb4C3
y = 9.8×10^5x + 2.0×10^4
R^2 = 0.9998
93Nb CyTOF Intensity
93Nb Concentration (ug/mL)
Mo2Ti2C3
y = 9.0×10^4x + 7.0×10^4
R^2 = 0.9999
95Mo CyTOF Intensity
95Mo Concentration (ug/mL)
Ta4C3
y = 7.1×10^6x – 3.4×10^5
R^2 = 0.9999
181Ta CyTOF Intensity
181Ta Concentration (ug/mL)
93Nb standard curve
95Mo standard curve
181Ta standard curve
c
CyTOF Intensity
93Nb
95Mo
140Ce
142Ce
151Eu
153Eu
165Ho
175Lu
181Ta
193Ir
Mass spectrum (m/z)

Figure S15. MXene quantification determined by CyTOF. a, Number of ^{93}Nb, ^{95}Mo, and ^{181}Ta atoms per cell determined from direct atom analysis in all PBMC subpopulations after the 24 h treatment of PBMCs with a cocktail of Nb_4C_3-260 nm, $Mo_2Ti_2C_3$-240 nm, and Ta_4C_3-160 nm (50 µg/mL each). **b,** Dynamic range of ^{93}Nb, ^{95}Mo, and ^{181}Ta determined by CyTOF solution mode. **c,** mass spectrum of Nb_4C_3, $Mo_2Ti_2C_3$ or Ta_4C_3 determined by CyTOF solution mode, lanthanide element calibration beads were applied as controls. All the experiments were performed in triplicate and shown as means±SD (One-way ANOVA, followed by Tukey's post hoc multiple comparison).

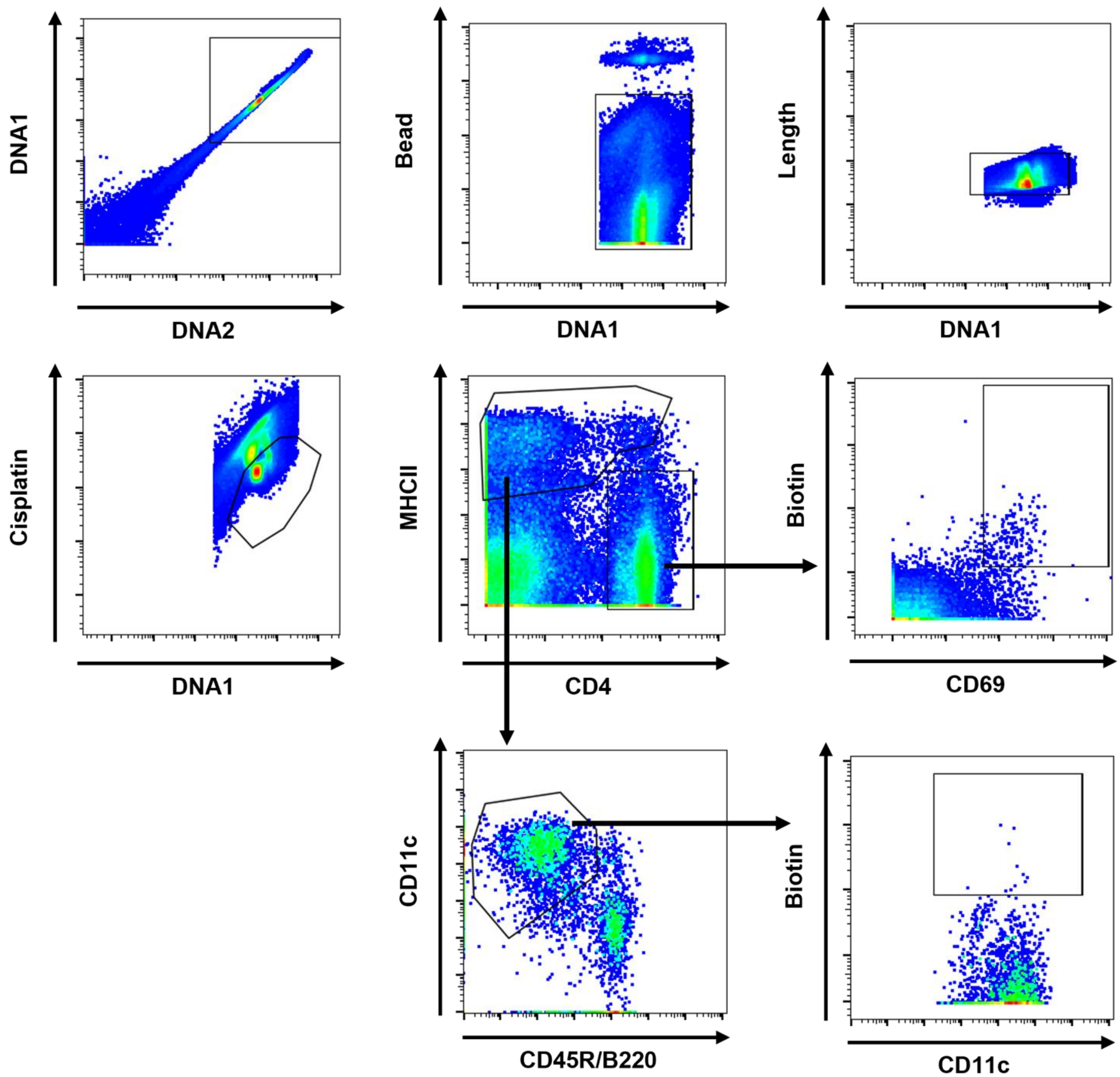

Figure S16. After singlets' and live/dead discrimination, T cells were identified as MHCII^{-}, CD4^{+} cells, while DCs as MHCII^{+}, CD4^{-}, CD11c^{+}, B220^{-}. CD69 was implemented as a marker of T cell activation. LIPSTIC labeling was then assessed in both cell populations.

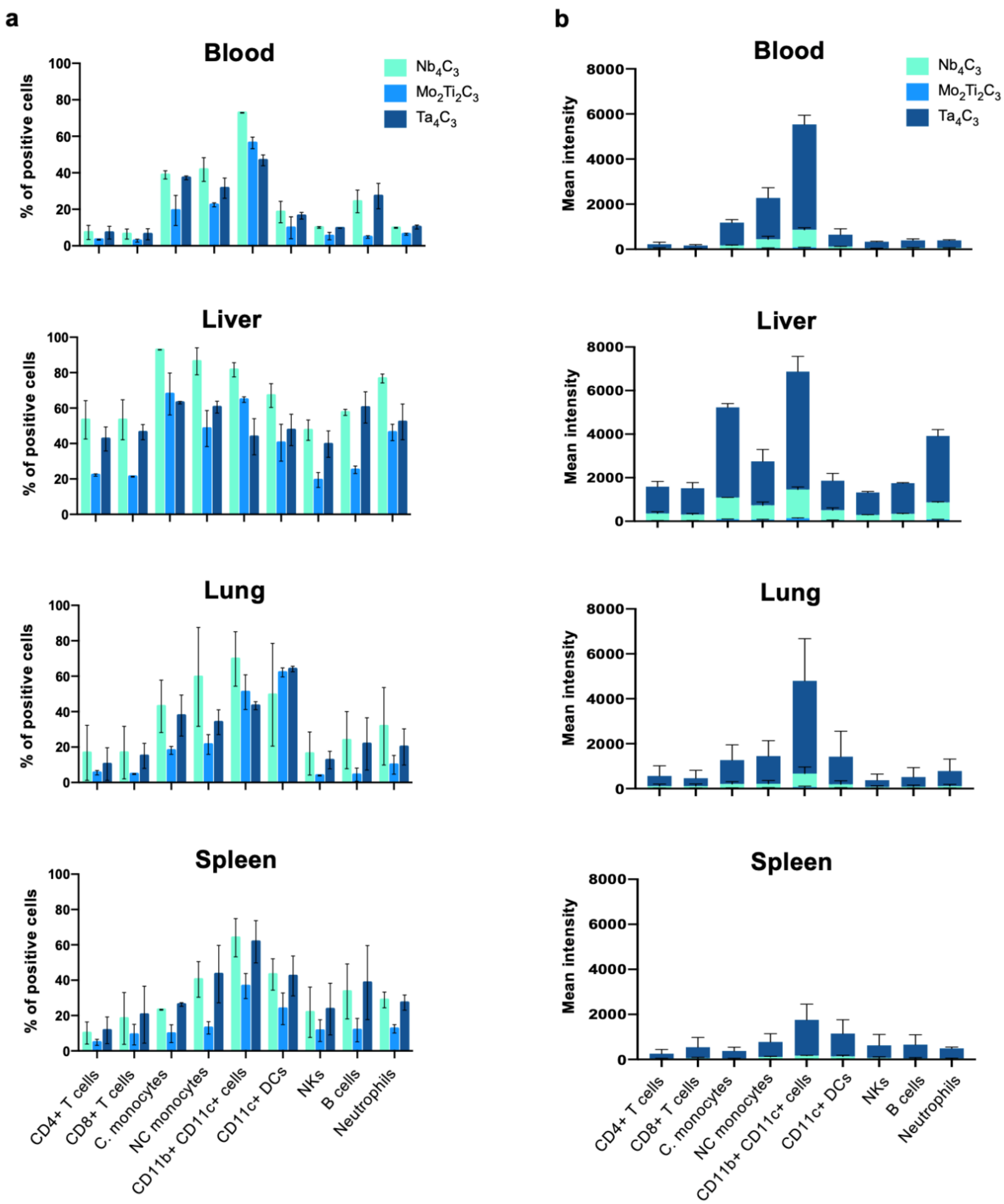

Figure S17. ***In vivo*** **biodistribution of MXene cocktail at the tissue and single-cell level. a**, Percentage of positive cells subtracted to control for all immune cell subpopulations identified per organ reported as bar graphs. **b,** MXene mean intensity for all immune cell subpopulations identified per organ reported as histograms. Data are presented as mean ± SEM among the replicates.

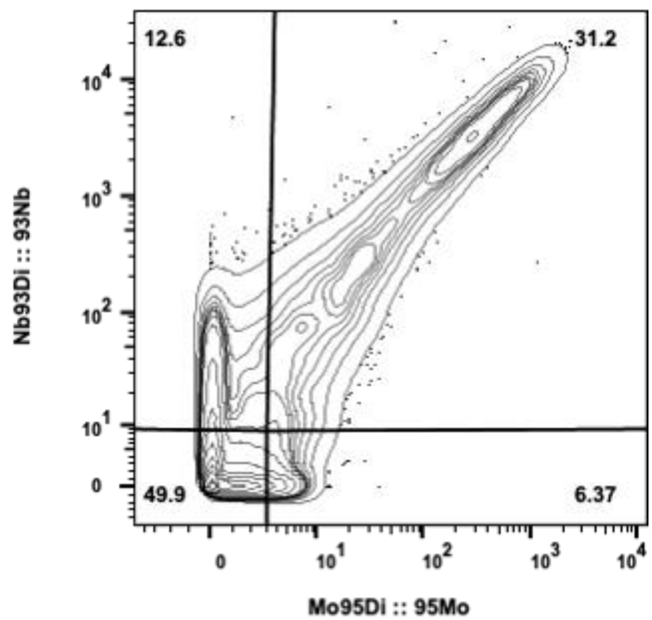

Figure S18. ***In vivo*** **biodistribution of MXene cocktail.** Representative contour plot of gated CD45+ cells, isolated from liver of MXene-treated mice.

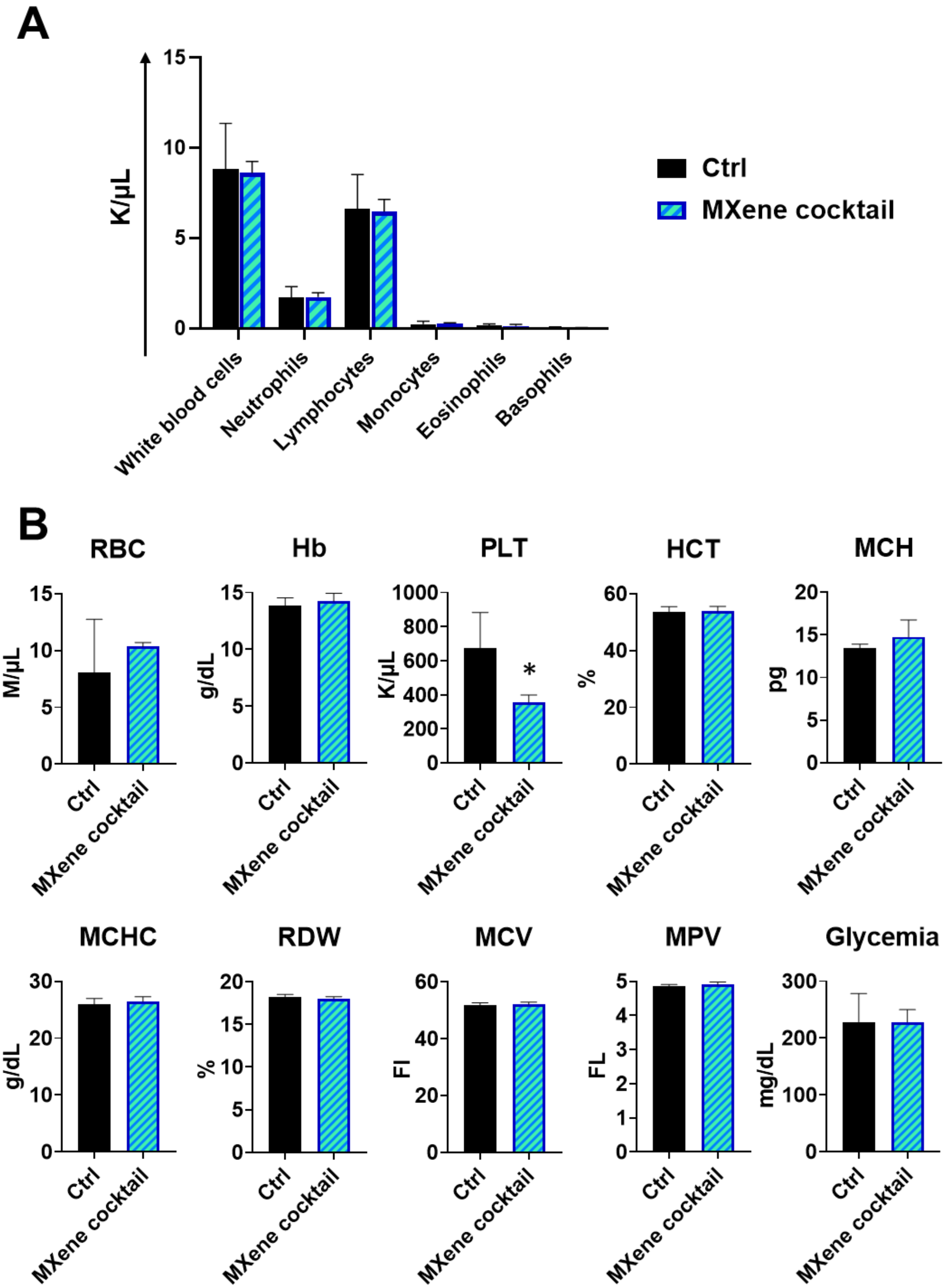
A
K/μL
15
10
5
0
White blood cells
Neutrophils
Lymphocytes
Monocytes
Eosinophils
Basophils
Ctrl
MXene cocktail
B
RBC
M/μL
Hb
g/dL
PLT
K/μL
*
HCT
%
MCH
pg
MCHC
g/dL
RDW
%
MCV
Fl
MPV
FL
Glycemia
mg/dL
Ctrl
MXene cocktail

Figure S19. *In vivo* effects of MXene cocktail on mice blood. Changes in human whole blood after treatment with Ctrl (Saline) or MXene cocktail and housed for 24 h. After 24 h, complete blood counts were performed. **a,** Changes in the number of total white blood cells (WBC), divided into neutrophils, lymphocytes, monocytes, eosinophils, and basophils, were analyzed. **b,** Changes in red blood cells (RBC), amount of hemoglobin (Hb), platelets (PLT), hematocrit (HCT), mean corpuscular hemoglobin (MCH) and its concentration (MCHC), red blood cell distribution width (RDW) mean corpuscular volume (MCV), mean platelet volume (MPV) and glycemia were also monitored. Data are presented as mean ± SD. Values of MXene-treated samples were compared to the corresponding untreated control using unpaired t-test.

Target	Metal	Clone	Catalog #	Company
CD45	089Y	HI30	201325	Fluidigm
CD196/CCR6	141Pr	G034E3	201325	Fluidigm
CD235a/b	141Pr	HIR2	201304	Fluidigm
IL-4	142Nd	MP4-25D2	3142002B	Fluidigm
CD19	142Nd	HIB19	201304	Fluidigm
CD123 (IL-3R)	143Nd	6H6	201325	Fluidigm
IL-5	143Nd	TRFK5	201308	Fluidigm
CD19	144Nd	HIB19	201325	Fluidigm
IL-4	144Nd	MP4-25D2	201308	Fluidigm
CD4	145Nd	RPA-T4	201325	Fluidigm
CD8a	146Nd	RPA-T8	201325	Fluidigm
CD11c	147Sm	Bu15	201325	Fluidigm
CD20	147Sm	2H7	201304	Fluidigm
CD16	148Nd	3G8	201325	Fluidigm
CD45RO	149Sm	UCHL1	201325	Fluidigm
CD66	149Sm	CD66a-B1.1	201304	Fluidigm
CD45RA	150Nd	HI100	201325	Fluidigm
MIP1β	150Nd	D21-1351	201308	Fluidigm
CD161	151Eu	HP-3G10	201325	Fluidigm
CD123	151Eu	6H6	201304	Fluidigm
CD194/CCR4	152Sm	L291H4	201325	Fluidigm
TNFα	152Sm	Mab11	201308	Fluidigm
CD25	153Eu	BC96	201325	Fluidigm
CD27	154Sm	O323	201325	Fluidigm
CD45	154Sm	HI30	201304	Fluidigm
CD57	155Gd	HCD57	201325	Fluidigm
CD183/CXCR3	156Gd	G025H7	201325	Fluidigm
IL-6	156Gd	MQ2-13A5	201308	Fluidigm
CD185/CXCR5	158Gd	J252D4	201325	Fluidigm
IL-2	158Gd	MQ1-17H12	201308	Fluidigm
GM-CSF	159Tb	BVD2-21C11	3159008B	Fluidigm
CD11c	159Tb	Bu15	201304	Fluidigm
CD28	160Gd	CD28.2	201325	Fluidigm
CD14	160Gd	M5E2	201304	Fluidigm
CD38	161Dy	HB-7	201325	Fluidigm
CD56 (NCAM)	163Dy	NCAM16.2	201325	Fluidigm
TCRgd	164Dy	B1	201325	Fluidigm
IL-17A	164Dy	N49-653	201308	Fluidigm
IFNg	165Ho	B27	3165002B	Fluidigm
CD61	165Ho	VI-PL2	201304	Fluidigm
IL-17F	166Er	SHLR17	201308	Fluidigm
CD27	167Er	O323	201304	Fluidigm
CD294 (CRTH2)	166Er	BM16	201325	Fluidigm
CD197/CCR7	167Er	G043H7	201325	Fluidigm
CD14	168Er	63D3	201325	Fluidigm
FNγ	168Er	B27	201308	Fluidigm
CD45RA	169Tm	HI100	201304	Fluidigm
CD3	170Er	UCHT1	201325	Fluidigm
CD20	171Yb	2H7	201325	Fluidigm
Granzyme B	171Yb	GB11	201308	Fluidigm

CD66b	172Yb	G10F5	201325	Fluidigm
CD38	172Yb	HIT2	201304	Fluidigm
HLA-DR	173Yb	LN3	201325	Fluidigm
IgD	174Yb	IA6-2	201325	Fluidigm
HLA-DR	174Yb	L243	201304	Fluidigm
TNFa	175Lu	Mab11	3175023B	Fluidigm
Perforin B	175Lu	D48	201308	Fluidigm
CD127 (IL-Ra)	176Yb	A019D5	201325	Fluidigm
DNA	191Ir	n/a	201192B	Fluidigm
DNA	193Ir	n/a	201192B	Fluidigm
Cisplatin Viability	195Pt	n/a	201064	Fluidigm

Table S1. Antibody conjugation for CyTOF analysis. A summary of antibodies, staining and conjugated metals used for CyTOF analysis.

Target	Metal	Clone	Catalog #	Company
I-A/I-E	209Bi	M5/114.15.2	3209006B	Fluidigm
CD45R/B220	176Yb	RA36B2	3176002B	Fluidigm
CD11c	162Dy	N418	3162017B	Fluidigm
CD69	143Nd	H1.2F3	3143004B	Fluidigm
CD4	172Yb	RM4-5	3172003B	Fluidigm
biotin	150Nd	1D4-C5	3150008B	Fluidigm

Table S2. Antibody conjugation for LIPSTIC analysis. A summary of antibodies, staining and conjugated metals used for LIPSTIC analysis.

Target	Metal	Clone	Catalog #	Company
CD45	89Y	30-F11	3089005B	Fluidigm
Ly-6C	150Nd	HK1.4	128002	Biolegend
CD11c	142Nd	N418	3142003B	Fluidigm
TCR-b	143Nd	H57-597	3143010B	Fluidigm
CD11b	148Nd	M1/70	101202	Biolegend
CD19	145Nd	6D5	115502	Biolegend
CD8a	146Nd	53-6.7	3153012B	Fluidigm
NK1.1	165Ho	PK136	108702	Biolegend
CD4	172Yb	RM4-5	3172003B	Fluidigm
CD117	173Yb	2B8	3173004B	Fluidigm
Ly-6G	141Pr	1A8	127602	Biolegend
DNA	191Ir	n/a	201192B	Fluidigm
DNA	193Ir	n/a	201192B	Fluidigm
Cisplatin Viability	195Pt	n/a	201064	Fluidigm

Table S3. **Antibody conjugation for *in vivo* biodistribution analysis.** A summary of antibodies, staining and conjugated metals used for *in vivo* biodistribution analysis.

Antibody target	Clone	Source	Cat#	Conjugated metal	Concentration (µg/mL)	Incubation conditions
CD3	SP162	abcam	ab245731	159Td	1.67	4˚C overnight
CD31	EPR17259	abcam	ab225883	174yb	2.5	4˚C overnight
CD74	In1/CD74	Biolegend	151002	172Yb	2.5	4˚C overnight
COL1A1	E8F4L	CST	72026	113In	1.25	4˚C overnight
dsDNA	35I9 DNA	Ionpath	708901	89Y	0.375	RT, 1 hour
F4/80	D2S9R	CST	70076	161Dy	10	4˚C overnight
Na-K-ATPase	EP1845Y	Ionpath	717603	176Yb	1	4˚C overnight
SMA	SP171	abcam	ab242395	115Ln	0.5	RT, 1 hour
Vimentin	D21H3	CST	5741	168Er	1.25	4˚C overnight

Table S4. Antibody conjugation for MIBI-TOF analysis. A summary of antibodies, staining concentrations and conjugated metals used for MIBI-TOF analysis.